Precambrian Research 182 (2010) 402–412

Contents lists available at ScienceDirect

Precambrian Research

journal homepage: www.elsevier.com/locate/precamres

Radiometric and stratigraphic constraints on terminal Ediacaran (post-Gaskiers) glaciation and metazoan evolution

Craig L. Hebert[a], Alan J. Kaufman[a,b,*], Sarah C. Penniston-Dorland[a], Aaron J. Martin[a]

[a] Geology Department, University of Maryland, College Park, MD 20742-4211, United States
[b] Earth System Science Interdisciplinary Center, University of Maryland, College Park, MD, United States

ARTICLE INFO

Article history:
Received 5 October 2009
Received in revised form 7 July 2010
Accepted 15 July 2010

Keywords:
Ediacaran Period
U/Pb zircon ages
Chemostratigraphy
Glaciation
Fauquier Formation
Catoctin Formation

ABSTRACT

Radiometric constraints on mid-Ediacaran Period glaciation (Gaskiers) in Newfoundland narrowed the known temporal gap between widespread ice ages and the evolution of complex metazoans to several million years. To further evaluate this claim we studied an Ediacaran glacial diamictite at the base of the Fauquier Formation of northern Virginia, and discovered a conformable relationship between the post-glacial cap carbonate and overlying volcanic rocks of the Catoctin Formation. U/Pb zircon age constraints for the rift-related volcanic flows suggest initial emplacement around 571 million years ago. Application of the Catoctin age to the Fauquier succession indicates the occurrence of an ice age about 10 million years younger than the 582 Ma Gaskiers event, supporting the view of multiple Ediacaran Period glaciations. Furthermore, the age constraint from eastern Laurentia falls within radiometric uncertainty of fossiliferous strata in Avalonia, indicating that the Fauquier glaciation was coincident with early metazoan evolution.

1. Introduction

Current radiometric and stratigraphic constraints suggest that the oldest complex Ediacaran fossils are separated by millions of years from the youngest recognized Neoproterozoic ice age deposits (Narbonne and Gehling, 2003). The timing of these events is important since extreme climate change has been considered a bottleneck to metazoan evolution (Hoffman et al., 1998; Hoffman and Schrag, 2002). In Newfoundland, for example, only ~1.5 km of strata separate Gaskiers Formation diamictites (ca. 580 Ma: Bowring et al., 2003) from morphologically simple discs and complex fronds of Ediacaran aspect in the overlying Drook Formation. The relatively short stratigraphic distance between climatic and biological events suggests either rapid post-glacial origination or diversification of metazoans, or that Gaskiers refrigeration represented no substantive evolutionary barrier.

Due to the lack of temporal constraints on most terminal Neoproterozoic glacial deposits, the true distribution of Gaskiers ice age deposits is uncertain, leading some to suggest that this Ediacaran Period glaciation was regional and hence unrelated to global Cryogenian events (i.e. 'snowball Earth': Hoffman et al., 1998). Before radiometric constraints were available for the Gaskiers diamictites, these glacial deposits on the Avalon microcontinent were typically equated with those of the Roxbury Formation (Squantum 'Tillite') preserved in the Boston Basin, USA, which is dated by U/Pb zircon analysis of a volcanic cobble near the base of the unit and of detrital zircons in underlying sandstone to be younger than ca. 595 Ma (Thompson and Bowring, 2000). If Squantum glaciation were contemporaneous with arc magmatism in the Boston Basin as suggested by these authors, then the Gaskiers and Roxbury ages are incompatible, suggesting the possibility of multiple Ediacaran Period ice ages (Fig. 1).

Other potential Ediacaran-age diamictites include those in the Mortensnes Formation of Norway (Halverson et al., 2005), the Egan Formation in Australia (Corkeron and George, 2001), the Hankalchough Formation in China (Xiao et al., 2004), and the Serra Azul Formation in Brazil (Alvarenga et al., 2007), although none of these examples are constrained by radiometric dates. Similar to the Gaskiers Formation (Myrow and Kaufman, 1999), post-glacial carbonate lithofacies (i.e. 'cap carbonates') above these examples preserve negative $\delta^{13}C$ anomalies, which, although of variable magnitude, have been provisionally correlated to a profound Ediacaran carbon cycle perturbation recognized worldwide and termed the Shuram event (Fike et al., 2006; McFadden et al., 2008).

Our studies in northern Virginia document a unique conformable relationship between glacial diamictite and cap carbonate of the Fauquier Formation with volcanic rocks of the Catoctin Formation, a widespread flood basalt recognized throughout eastern North America that was emplaced during the prolonged rifting of

* Corresponding author at: Geology Department, University of Maryland, College Park, MD 20742-4211, United States. Tel.: +1 301 405 0395; fax: +1 301 405 3597.
E-mail address: kaufman@geol.umd.edu (A.J. Kaufman).

0301-9268/$ – see front matter © 2010 Elsevier B.V. All rights reserved.
doi:10.1016/j.precamres.2010.07.008

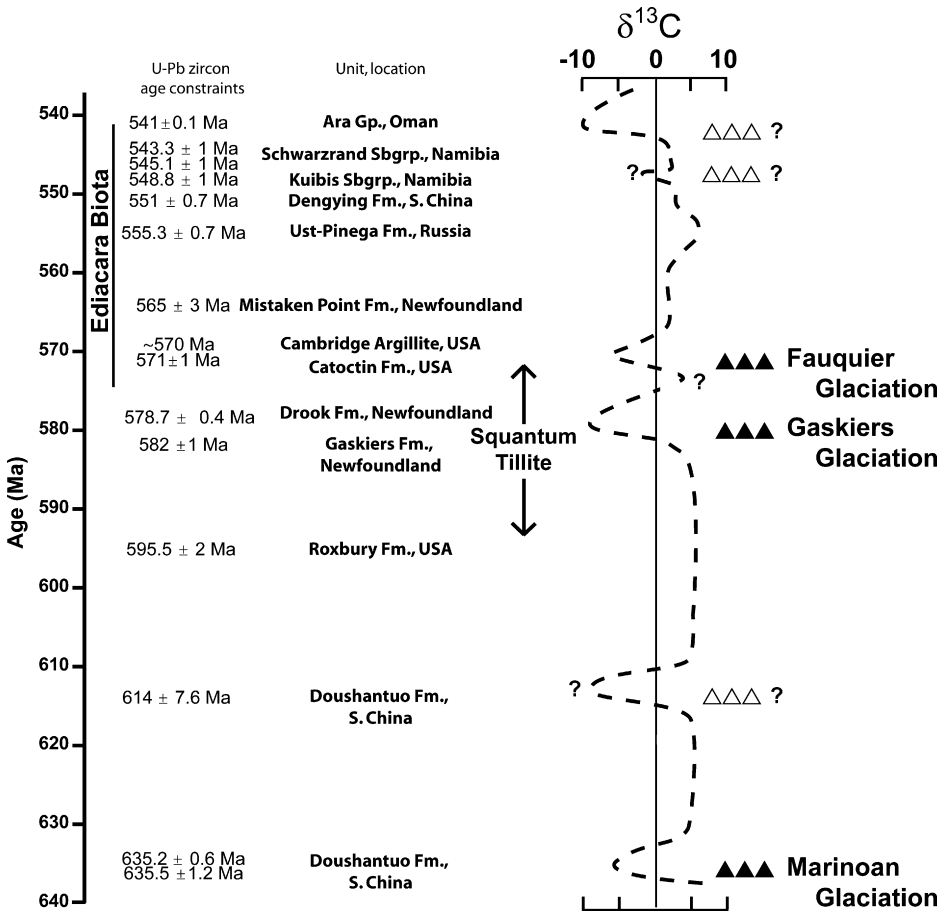

Fig. 1. Radiometric constraints on Ediacaran Period climatic, biological, and carbon-isotope events. U/Pb zircon ages from Aleinikoff et al. (1995), Bowring et al. (2003, 2007), Thompson and Bowring (2000), Grotzinger et al. (1995), Condon et al. (2005), Martin et al. (2000), Benus (1988), Hoffmann et al. (2004), Hoffman and Li (2009), Liu et al. (2009), and Southworth et al. (2009). Composite of Ediacaran Period carbon-isotope stratigraphy from Kaufman et al. (1991, 1993, 1997), Pelechaty et al. (1996), Saylor et al. (1998), Bartley et al. (1998), Jiang et al. (2007), and McFadden et al. (2008). Filled triangles represent positions of known glacial deposits and open triangles indicate the stratigraphic position of possible ice ages based on negative $\delta^{13}C$ excursions.

Laurentia from Amazonia and the formation of the Iapetus Ocean in the middle of the Ediacaran Period (Aleinikoff et al., 1995; Cawood et al., 2001; Li et al., 2008). Stratigraphic observations coupled to radiometric constraints on the Catoctin volcanic rocks indicate that the Fauquier ice age post-dates that of the Gaskiers, and further demonstrate that Ediacaran glaciation was broadly contemporaneous with metazoan evolution. Constraints from U/Pb isotopic ages of detrital zircons and the mineralogy of contact metamorphism support this interpretation.

2. Geologic setting

The middle to late Neoproterozoic was a time of rifting of the Baltic and Amazonian cratons from the northeastern and southeastern margins of Laurentia, respectively (Li et al., 2008). Early rifting began ca. 760 Ma, and final rifting and opening of the Iapetus Ocean took place between ca. 620 and 560 Ma (Aleinikoff et al., 1995; Cawood and Pisarevsky, 2006). There are conflicting published conclusions about the latitude of the eastern margin of Laurentia at the time of deposition of the Fauquier and Catoctin formations. Based on paleomagnetic data from the Catoctin volcanics, Meert et al. (1994) show this portion of Laurentia near the South Pole, whereas Pisarevsky et al. (2000) argue for latitudes in the southern tropics based on a paleopole for Siberia and a proposed connection with Laurentia in the Ediacaran Period.

The Fauquier Formation is part of the thick rift-related succession of igneous and sedimentary rocks in the eastern Blue Ridge of central and northern Virginia, USA (Fig. 2) recognized as the Lynchburg Group (Wehr, 1985; Wehr and Glover, 1985; Espenshade, 1986; Kasselas and Glover, 1997). In at least two laterally extensive localities, the upper Lynchburg Group (including the basal Fauquier Formation diamictite and equivalent Rockfish Conglomerate: Wehr, 1986) lies unconformably above ca. 1.1 Ga Mesoproterozoic basement rocks (Parker, 1968; Espenshade, 1986; Davis et al., 2001; Southworth et al., 2008) (see Fig. 4). The Rockfish Conglomerate contains outsized basement clasts in fine-grained rhythmites, interpreted as ice-rafted dropstones (Wehr, 1986), whereas the basal Fauquier Formation in our study area contains both rounded and angular cobbles and boulders in coarse, cross-bedded sandstone (Fig. 3A and B), which we interpret as pro-glacial fluvial outwash facies (*cf.* Bailey and Peters, 1998). The basal diamictite in each area is overlain by thick, immature basin-filling siliciclastic rocks. In the Rockfish River area (Fig. 4) these are primarily composed of greywacke and argillite of the Thoroughfare Mountain, Ball Mountain, and Charlottesville formations, which accumulated as turbidites and gravity flow deposits in a deep marine environment (Brown, 1970; Wehr, 1985). Equivalent units of the Fauquier Formation in our study area (including the thin Swift Run sedimentary package present on the western side of the Blue Ridge anticlinorium: Fig. 2) are composed of coarse arkose and pebbly sandstones, suggesting a shallower proximal marine to fluvial setting, followed by calcareous siltstone and then a regionally persistent but thin (<20 m thick) carbonate (Espenshade, 1986; Wehr, 1986; Kasselas, 1993).

The lower Lynchburg Group in central Virginia also includes glacial deposits of the 702–705 Ma Mechum River (Tollo and

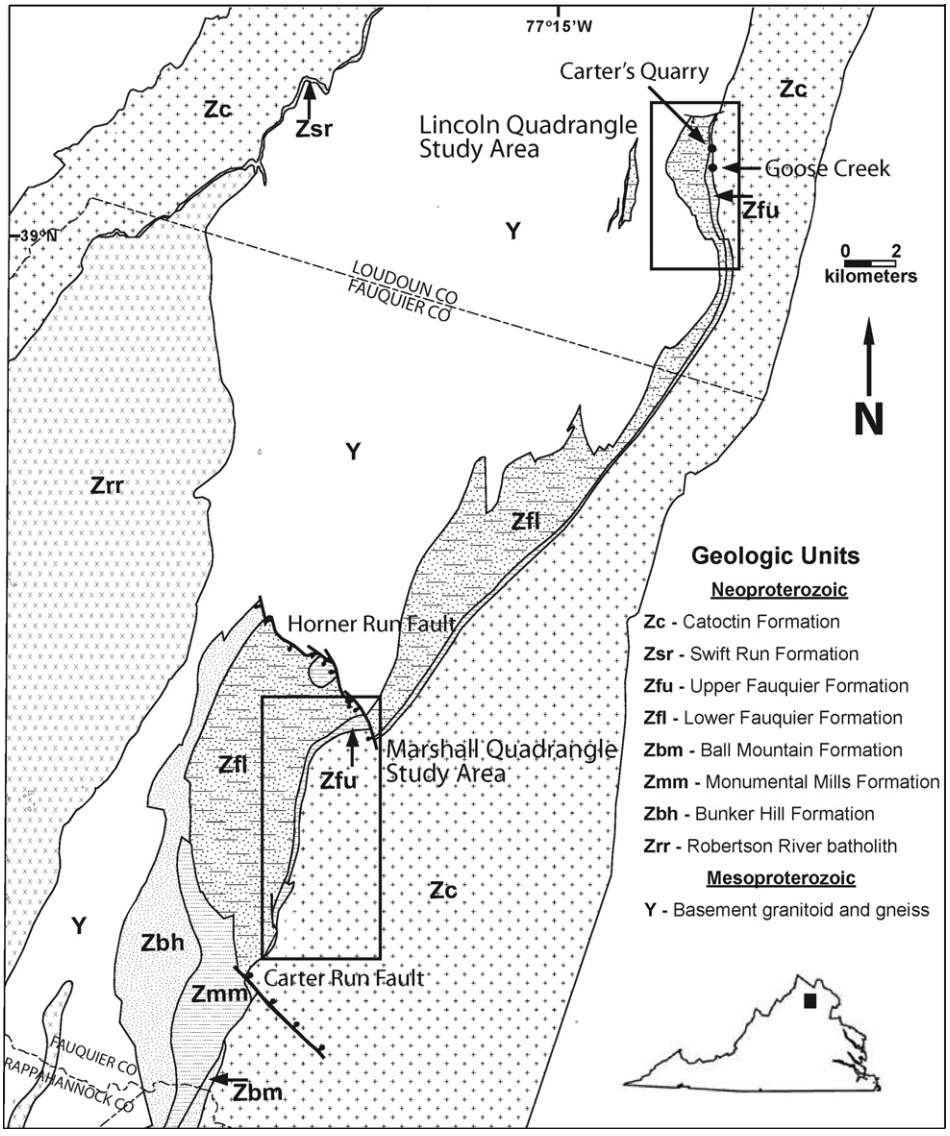

Fig. 2. Map of northern Virginia outcrop area (modified from Davis et al., 2001).

Hutson, 1996; Bailey and Peters, 1998) and equivalent Bunker Hill formations. These are overlain by argillite of the Monument Mills Formation, which lies unconformably beneath the Fauquier diamictite in the Warrenton, Virginia area. Immediately north of the Carter Run fault (Fig. 2: Kasselas, 1993) the Fauquier glacial deposits sit on top of the Bunker Hill Formation, and in the northern portion of our field area the diamictite sits on ca. 1.1 Ga meta-granite, suggesting variable degrees of sub-glacial erosion (see Fig. 4 for regional correlations).

3. Results

3.1. Field observations

The boulder bed at the base of the Fauquier diamictite is primarily composed of outsized clasts of basement granite and gneiss in a black to grey matrix of coarse sands and grits. While boulders decrease in abundance up section, the sandstones become progressively red in color (Fig. 3C) and have been previously described as 'red beds' (Kline et al., 1991). This is likely the result of oxidation of remarkably high abundances of magnetite, which we observed in thin sections and during separation of detrital zircons. The pro-glacial fluvial sandstones and conglomerates give way to rhythmic calcareous siltstone and then shallow marine limestone. In the Marshall area, bedding structures in the limestone include a basal intra-formational breccia followed by finely laminated rhythmite, ribbon rock (Fig. 3E), microbialaminites and stromatolites.

Sedimentary structures in the upper reaches of the carbonate in the Lincoln Quadrangle are generally lost due to recrystallization associated with the emplacement of the Catoctin flood basalt. At Carters Quarry (Fig. 2) a 2-m thick basalt flow is inter-layered with the marble (*cf.* Wehr, 1985; Espenshade, 1986; Kline et al., 1991; Kasselas and Glover, 1997; Aleinikoff et al., 1995, Southworth et al., 2006, 2008), and in a nearby quarry along Goose Creek we found evidence of pillow basalt interaction with wet carbonate sediment. In this shallow marine environment it appears the carbonate sediments were squeezed and contorted into diapirs between the basalt pillows (Fig. 3G), and rapid volatilization of pore water shattered the underlying carbonate forming a hyaloclastic texture (Fig. 3F). A similar interpretation was made based on the presence of sedimentary dikes projecting up into overlying Catoctin greenstone farther south by Reed (1955), who interpreted that they formed due to the flow of basalt over wet sediment.

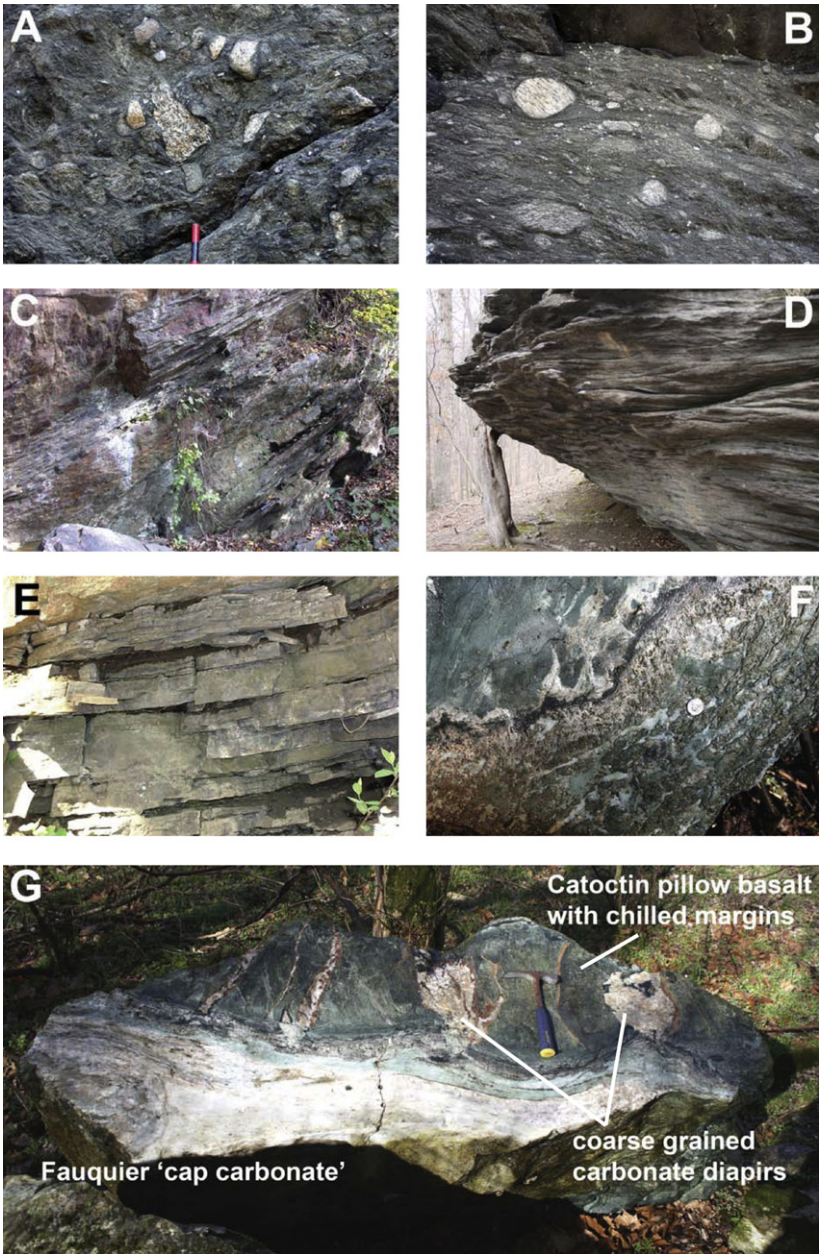

Fig. 3. Field photographs of the Fauquier and Catoctin formations in northern Virginia (Aldie) along Goose Creek including, (A) boulder bed diamictite with a coarse magnetite-rich sandstone matrix and both rounded and angular clasts dominated by 1.1 Ga meta-granite; (B) rounded boulders at the base of the Fauquier Formation truncating cross-beds in coarse sandstone and in an interval of finely laminated siltstone; (C) red bed sandstone and granule conglomerate above the basal diamictite; (D) interval of granule conglomerate and coarse sandstone sampled for detrital zircon study; (E) ribbon limestone of the upper Fauquier Formation cap carbonate; (F) hyaloclastic texture at contact between the Catoctin meta-basalt and marble of the Fauquier cap carbonate, indicating that the sediments were water saturated during emplacement of the volcanic rocks; (G) basalt of the Catoctin Formation with diapirs (flame structures) of Fauquier carbonate injected between the chilled margins of the pillows.

The marble diapirs are coarsely crystalline and reaction rims contain relatively coarse-grained grossular garnet, chlorite, actinolite, epidote, magnetite, calcite, and dolomite as determined by powder XRD analyses. The original protolith mineralogy of the basalt was likely dominantly plagioclase and clinopyroxene (Badger and Sinha, 1988; Badger, 1993), while the original protolith mineralogy of the carbonate sediments was likely calcite(aragonite) ± dolomite. Minerals that developed in the Catoctin basalt during greenschist facies metamorphism include albite, chlorite, epidote, actinolite, and quartz (Reed, 1955; Badger, 1993). Garnet (grossular) is the only mineral in these rims that is not reported in either the Catoctin basalt or the Fauquier Formation and most likely formed during contact metamorphism of the protolith (due to reaction between plagioclase and clinopyroxene of the basalt and calcite of the limestone) in the presence of fluids. However, it is also possible that garnet formed during later Paleozoic greenschist facies metamorphism. The main difference between the two scenarios would be the potential temperatures of reaction, with higher temperatures attained during contact metamorphism relative to regional metamorphism.

Three possible end-member grossular-producing reactions from the original protolith minerals are:

$$5Di + 12Cal + 10An + 4H_2O = Chl + 9Gr + 12CO_2 \quad (A)$$

$$2An + 4Cal + Di = 2Gr + Dol + 2CO_2 \quad (B)$$

$$An + 2Cal + Di = Qtz + Gr + Dol \quad (C)$$

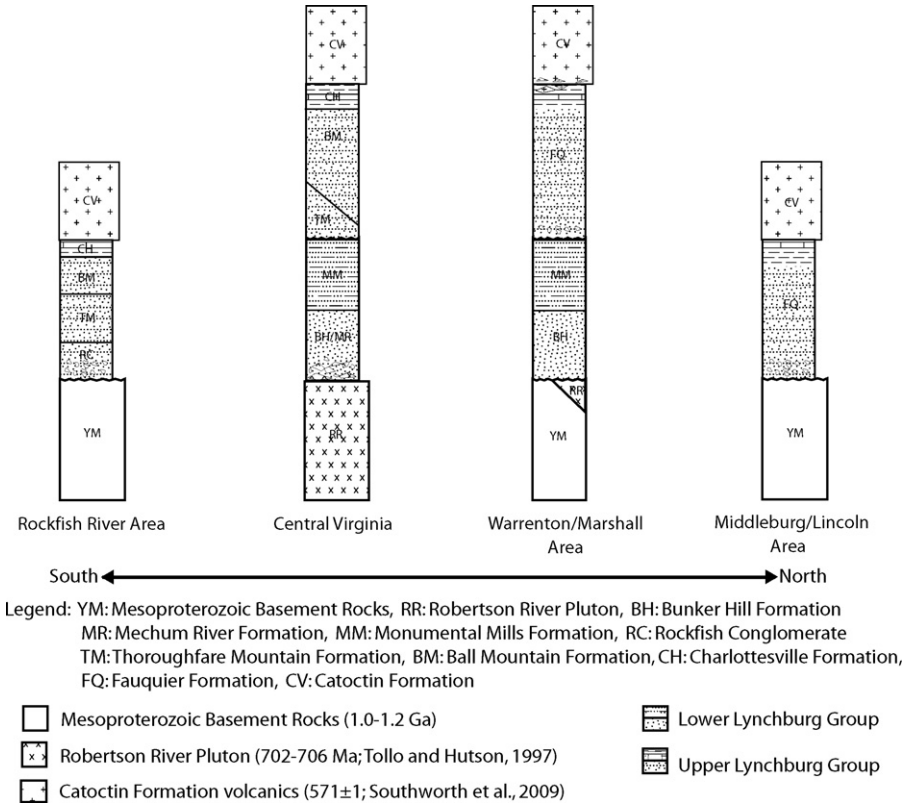

Fig. 4. Generalized central and northern Virginia Eastern Blue Ridge Neoproterozoic stratigraphy.

where An = anorthite, Cal = calcite, Chl = chlorite, Di = diopside, Dol = dolomite, Gr = grossular, and Qtz = quartz. Phase diagrams (Fig. 5) were produced for pure Mg end members to evaluate the range of temperatures of reaction. To evaluate the effect of adding Fe to the system on equilibrium temperature, simplified mineral equilibria (assuming constant molar volume) were calculated for reaction C using both Mg and Fe end-members (ankerite and hedenbergite instead of dolomite and diopside) and the difference was evaluated over the range of up to 5 kbar pressure using thermodynamic data from Holland and Powell (1998). Calculations of mineral equilibria using Fe end-member mineral compositions increased the equilibrium temperature by only ~60–65 °C. These calculations indicate that grossular-producing reactions occur over a wide range of temperatures at low pressures and are possible both in the presence or absence of fluids. This suggests that garnet could have formed during contact metamorphism between the basalt and wet carbonate sediments, however we cannot rule out the formation of garnet along this contact during later greenschist facies metamorphism.

3.2. Stable isotope geochemistry

Fig. 6 illustrates our results of carbon and oxygen isotope analyses of upper Fauquier Formation carbonates from the Marshall and Lincoln quadrangles (Table 1). In the Marshall Quadrangle, primary structures in the organic-rich microspar limestone are well preserved, consistent with lower greenschist facies regional metamorphism (Espenshade, 1986). To the northeast, however, towards the Lincoln Quadrangle, most carbonates are organic-poor and are generally recrystallized to a sugary marble; samples adjacent to basalt contacts are extremely coarse grained (up to 0.5 cm).

Petrographic and CL observation of thin sections and billets guided our drilling of the least altered and finest grained carbonate phases in these samples. Resulting powders were reacted with anhydrous phosphoric acid ($\rho > 1.89$ g/ml) for 10 min with a MultiCarb reaction device; evolved CO_2 was cryogenically separated from H_2O and introduced into the dual inlet of a GV Isoprime mass analyzer. Uncertainties based on multiple ($n > 8$) analyses of a standard carbonate powder (NBS-19) interspersed throughout the analytical session were better than 0.05‰ (1σ) for both C and O isotopes.

The composite stratigraphy reveals a strong positive $\delta^{13}C$ excursion over ~20 m of section from −6.6‰ at the base to as high as +4.6‰ near the upper contact with the Catoctin volcanic rocks. The negative $\delta^{13}C$ values and overall carbon-isotope trend are consistent with those of Neoproterozoic cap carbonates worldwide (Kaufman and Knoll, 1995; Kennedy, 1996; Hoffman et al., 1998) supporting the glacial interpretation of the basal Fauquier diamictite. Oxygen isotopes in the lower interval from organic-rich limestone samples in the Marshall Quadrangle are remarkably consistent, with values ranging between −10 and −12‰, but are considerably more variable in the marble samples collected at Carter's Quarry in the Lincoln Quadrangle. This variability likely reflects high temperature recrystallization of the carbonate in the presence of an aqueous fluid during contact metamorphism. This interpretation is supported by the greater depletion in ^{18}O immediately below the basalt flow and also recorded in coarse-grained carbonate diapirs (Fig. 7).

3.3. Detrital zircon geochronology

In order to constrain the maximum depositional age of the Fauquier Formation, we obtained U/Pb isotopic ages of detrital zircons from poorly sorted sandstone to granule conglomerate stratigraphically below the calcareous siltstone and cap carbonate at the Goose Creek section in the Lincoln Quadrangle of Loudon County (Table S1). Approximately two kilograms of the sample were pulverized by hand to disaggregate grains. Zircons were sepa-

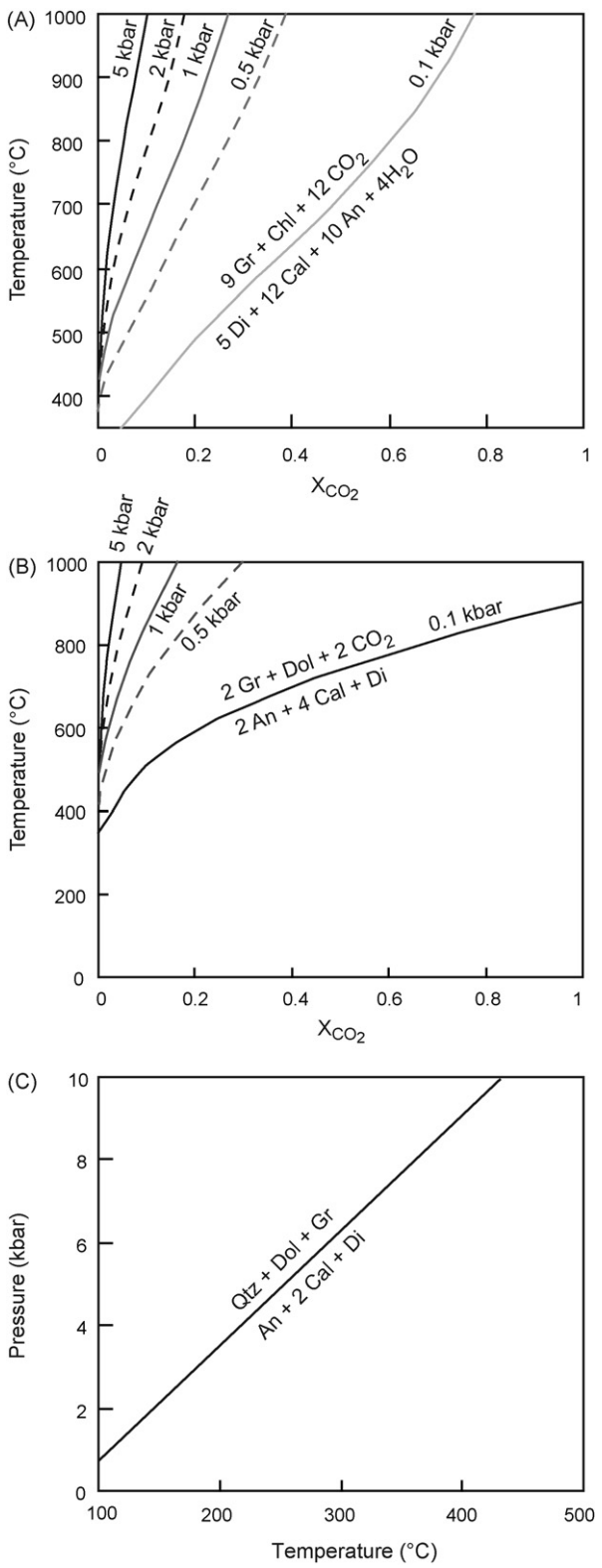

Fig. 5. Calculated mineral equilibria for reactions A, B, and C. Calculations were performed using the software package TWEEQU (Berman and Brown, 1992), assuming end-member Mg mineral compositions. An = anorthite, Cal = calcite, Chl = chlorite, Di = diopside, Dol = dolomite, Gr = grossular, Qtz = quartz. (A) Temperature – X_{CO_2} diagram showing mineral equilibria for reaction A at different pressures. Reaction does not require temperatures greater than 350 °C for $P < 5$ kbar. B. Temperature – X_{CO_2} diagram showing mineral equilibria for reaction B at different pressures. Reaction does not require temperatures greater than 400 °C for $P < 5$ kbar. C. Pressure-Temperature diagram showing mineral equilibrium for reaction C. Reaction does not require temperatures greater than 350 °C for $P < 5$ kbar.

rated by density using water and methylene iodide and by magnetic susceptibility using a Frantz magnetic barrier separator. All analyzed zircons were non-magnetic at 2 amps, a side tilt of 20°, and a forward tilt of 10°. There was a large amount of magnetite in the sand-size fraction. Zircon grains were poorly sorted, with a wide range of sizes. Part of the zircon separate was poured onto a piece of double-sided tape for mounting in epoxy. Pouring the zircons removed the possibility of biasing the sample during hand-picking of grains, an alternative method for mounting grains. Several shards of a standard zircon were included in the mount, and all grains were located no more than 5 mm from the center of the mount. Each mounted grain was imaged by both backscattered electrons and cathodoluminescence (CL) using the JEOL JXA-8900R electron probe microanalyzer at the University of Maryland and the images were used to guide the placement of the laser spots during mass spectrometry to avoid cracks, inclusions, and multiple CL zones.

^{238}U, ^{232}Th, ^{207}Pb, ^{206}Pb, and ^{204}Pb were measured using a GV Instruments Isoprobe multi-collector – inductively coupled plasma – mass spectrometer at the Arizona LaserChron Center in the University of Arizona. This machine was attached to a 193 nm Excimer laser that ablated zircon from a spot with a diameter of 35 μm. The ablated material was carried into the plasma in He gas. Grains were selected for analysis sequentially by position in the mount with no regard for shape, size, or brightness or zoning type in the CL images. Only zircon cores were analyzed to avoid possible rims grown during metamorphism of the Fauquier Formation. Analyses of the zircon standard bracketed analysis of every five unknown grains. We followed the analysis and data reduction procedures in Gehrels et al. (2008) except that we relied on analyses more than 75% concordant. All analyses indicate ages older than 1 Ga, so we use exclusively $^{206}Pb/^{207}Pb$ dates as crystallization ages because these dates usually are more accurate than $^{206}Pb/^{238}U$ dates for such old grains.

Fig. 8 shows the results of the isotopic analyses; the 120 detrital zircons measured all yielded Grenvillian U/Pb ages between ca. 1020 and 1270 Ma with a broad peak at ca. 1150 Ma. The youngest group of three or more age determinations is at ca. 1030 Ma, which we take as the maximum depositional age for the Fauquier Formation.

4. Discussion

Regional map and stratigraphic relationships suggest that the Fauquier succession accumulated in large response to the rapid infilling of glaciated valleys in nearshore shallow marine or terrestrial environments with coarse fluvial conglomerates and sands likely winnowed from moraines. While the thick siliciclastic interval between the boulder bed diamictite and the cap carbonate (Fig. 6) is unusual from a Cryogenian perspective, we suggest that this may be the expected sedimentary response in a rift-related setting where sediment accumulation rates can be remarkably high (Friedmann and Burbank, 1995). Post-glacial transgression ultimately inundated the shoreline, pushing back the source of siliciclastic sediments and allowing carbonate to accumulate in the shallow marine environment. It also seems possible that widespread eruption of the Catoctin volcanic rocks may have played a role in the shutdown of terrestrial inputs to the depositional basin.

The composite carbonate chemostratigraphy (Fig. 6) reveals a nearly 10‰ rise in $\delta^{13}C$ compositions defined by closely spaced samples over some 20+ m of section before the biogeochemical excursion is abruptly truncated by the Catoctin volcanic rocks. Such trends are typical of relatively organic-rich cap carbonates (*sensu* the grey Rasthof Formation vs. the pink Maieberg Formation in northern Namibia: Hoffman et al., 1998), and may be explained by a progressive increase in the proportional burial of organic matter

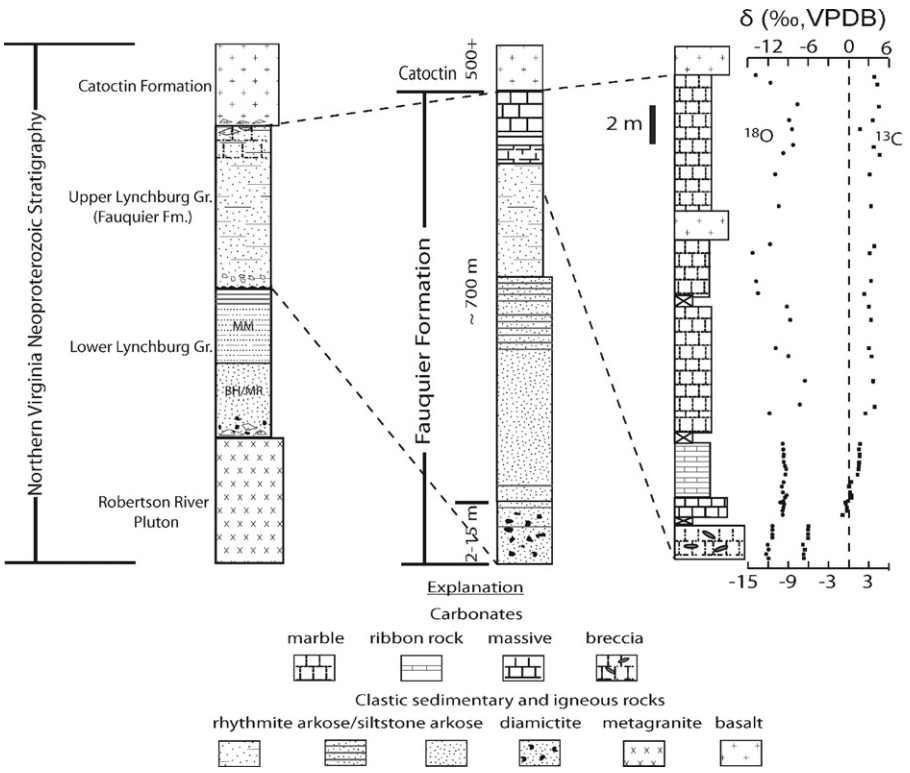

Fig. 6. Lithostratigraphy and chemostratigraphy of the Fauquier Formation carbonate in northern Virginia. The carbon-isotope trend from the base of the unit to the top of the carbonate reveals a greater than 10‰ positive excursion consistent with post-glacial cap carbonates worldwide. Thickness calculation of the Fauquier conglomerate and sandstone interval estimated from map relationships in the Lincoln Quadrangle. Our composite chemostratigraphy is based on samples from five measured sections.

(Hayes et al., 1983) associated with post-glacial primary productivity in the depositional basin. Total organic carbon contents of Fauquier carbonate range between 0.2 and 1.9 mg C/g sample, with the lowest values found in the marble samples from the Lincoln Quadrangle (Table 1). While the lowest $\delta^{13}C$ in the brecciated interval (−6.6‰) is typical of Cryogenian caps, carbonate in the underlying calcareous siltstone is even more depleted in ^{13}C (with values as low as −8.5 to −9.0‰) similar in composition to carbonate clasts in the uppermost Gaskiers diamictite (Myrow and Kaufman, 1999) and approaching the nadir in values recognized in the older Ediacaran Period Shuram anomaly recognized worldwide (Condon et al., 2005; Fike et al., 2006; Kaufman et al., 2007; McFadden et al., 2008).

While the upper Fauquier carbonate is significantly recrystallized, the overall carbon isotope trend that defines the positive $\delta^{13}C$ excursion remains coherent. Given its remarkable similarity to unmetamorphosed post-glacial examples it is likely that this reflects chemical changes in the depositional environment. This view is supported by the narrow range of $\delta^{18}O$ values in the carbonates, which is considerably smaller than that for carbon isotopes and

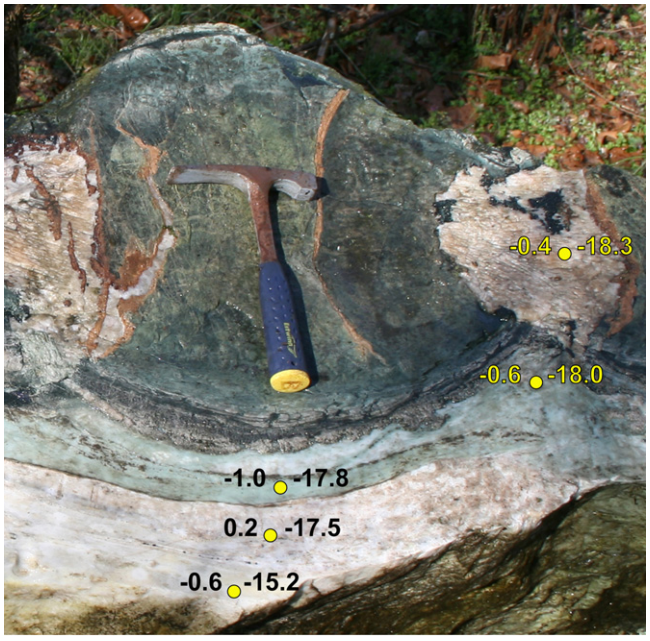

Fig. 7. Coarse carbonate diapir of the Fauquier carbonate intruding pillows of basal Catoctin Formation basalt. The values represent carbon (left) and oxygen (right) isotope compositions of the carbonate in each of the sub-sampled regions; see discussion of metamorphic reactions and associated mineralogies.

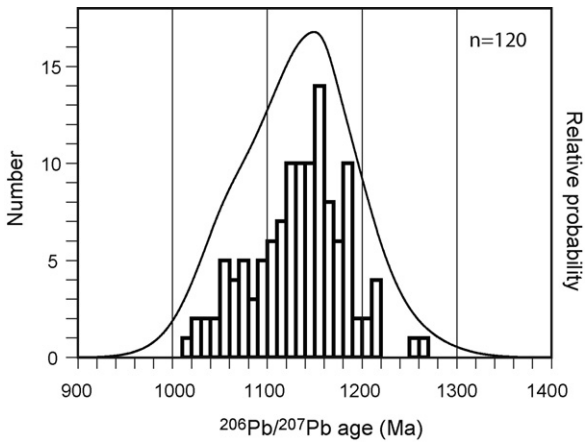

Fig. 8. Relative probability plot (solid line) and histogram (rectangles) for detrital zircon $^{206}Pb/^{207}Pb$ ages from the upper part of the Fauquier Formation. Histogram rectangles are 10 Ma wide. Relative probability is unit less.

Table 1
Carbon and oxygen isotopic data for Fauquier Formation carbonates.

Sample	δ^{13}Ccarb (‰, VPDB)	δ^{18}O (‰, VPDB)	Sample	δ^{13}Ccarb (‰, VPDB)	δ^{18}O (‰, VPDB)
Marshall Quadrangle Samples			Marshall Quadrangle Samples, con't		
Horner Run			*Wadlow Farm*		
(*calcareous siltstone - not shown on stratigraphic sections*)			98.4.0.40	1.31	−9.37
99.1.0.00	−8.49	−15.47	98.4.0.75	1.50	−9.37
99.1.0.75	−8.72	−16.27	98.4.1.00	1.59	−9.49
99.1.1.15	−8.57	−16.05	98.2.0.15	1.64	−9.71
99.2.0.55	−9.03	−17.86	98.2.0.45	1.70	−9.77
99.2.0.78	−8.42	−14.77	98.2.0.54	1.60	−9.65
99.3.0.89	−8.85	−17.51	98.2.0.80	1.58	−9.78
99.3.1.08	−8.42	−14.51	98.2.1.08	1.68	−9.82
99.3.1.15	−8.69	−16.53			
99.4.1.00	−8.37	−15.12	Lincoln Quadrangle Samples		
99.4.1.35	−8.77	−16.71	*Goose Creek*		
			GC1.0.0	2.51	−4.60
Halls Point			GC1.0.5	2.31	−8.75
HP1-3	−6.32	−12.05	GC1.1.5	2.54	−11.88
HP1-1	−6.49	−12.00	GC1.2.0	3.70	−7.41
HP1-2A	−6.45	−12.26	GC1.2.4	2.61	−10.11
HP1-2B	−6.12	−11.77	GC1.3.0	2.34	−8.08
HP2-0.5A	−6.56	−12.24	GC1.3.5	3.58	−6.67
HP2-0.5B	−5.78	−11.59	GC1.4.0	2.48	−8.07
HP2-1A	−6.56	−12.08	GC1.4.5	2.80	−4.75
HP2-1B	−6.02	−11.54	GC-5	3.30	−9.02
HP2-2A	−6.47	−12.35	GC-5.5	3.00	−11.05
HP2-2B	−6.40	−11.78	GC-7.5	3.29	−8.80
HP2-2D	−6.14	−11.72	GC-8.5	3.00	−9.28
HP2-1-0	−5.98	−11.51			
HP2-1-0.5	−5.92	−11.54	*Lime Kiln Road*		
HP2-1-2	−6.04	−11.48	LK1-.2	2.30	−13.72
HP2-1-2.5	−5.96	−11.44	LK1-1	3.33	−14.00
			LK1-3	3.09	−14.29
Enon Church			LK1-12	3.62	−11.79
6.0.00	−0.91	−9.90			
6.0.30	−0.25	−9.88	LK2-0	3.34	−10.49
6.0.50	−0.22	−9.79	LK2-2	3.10	−10.96
6.0.75	−0.40	−9.65	LK2-3.5	4.60	−9.85
98.1.0.75	−0.48	−10.18	LK2-4	3.72	−8.26
6.0.95	−0.08	−9.70	LK2-5	1.79	−8.46
98.1.1.25	0.46	−9.46	LK2-5.5	3.52	−8.95
6.1.35	0.47	−9.28	LK2-6.5	4.31	−7.68
98.1.1.75	0.18	−9.81	LK2-8	4.15	−11.77
98.1.2.25	0.07	−10.00	LK2-8.5	3.82	−13.84
98.1.2.50	0.41	−9.67			
			Goose Creek Quarry sub-samples		
			KD07-1	−0.55	−15.22
7.0.10	0.60	−9.06	KD07-2	0.17	−17.50
7.0.25	0.88	−9.28	KD07-3	−0.95	−17.77
7.0.60	0.80	−9.11	KD07-9	−0.33	−8.45
7.0.95	0.83	−9.17	KD07-15	−0.58	−17.99
7.1.10	0.77	−9.18	KD07-16	−0.04	−18.27
7.1.30	0.74	−8.10			
8.0.00	0.64	−9.84			
8.0.15	0.51	−9.95			

contrary to model expectations for diagenetic isotope exchange (Banner, 1995; Jacobsen and Kaufman, 1999). Clear alteration of δ^{18}O values is noted only in samples taken directly beneath basalt flows. While δ^{18}O compositions of the basal breccia beds are a few permil lighter than those in overlying horizons, it is possible that these values reflect significantly warmer seawater temperatures associated with high concentrations of atmospheric CO_2 in the post-glacial atmosphere (Bao et al., 2008). Although rarely discussed, significant δ^{18}O trends defined by closely spaced samples are also noted in Cryogenian cap carbonates, including the Maieberg Formation in northern Namibia, where the lowest oxygen isotope values appear to coincide with maximal transgression.

The Fauquier Formation cap carbonate is regionally overlain by basalt of the Catoctin Formation, and previous investigations have suggested the likelihood of a soft-sediment contact (e.g. Reed, 1955). Our observations in the Marshall Quadrangle support this view, although we acknowledge that the structures illustrated in Fig. 3G from an isolated block might have formed during later deformation and metamorphism. In this scenario, the basalt intruded lithified carbonate rock as a sill and during subsequent deformation weaker carbonate rock filled space between boudins. The garnet and other minerals were then produced during regional metamorphism. Our preferred interpretation, however, is that the observed structures, textures, and mineralogies are the result of the mobilization of water-saturated unconsolidated carbonate sediment during loading by an overlying basalt flow. In this scenario, the slurry of loose sediments, fluids, and volatiles were injected between lobes or pillows of the basalt as veins and diapirs; garnet and other metamorphic minerals formed along the periphery of these structures as a result of contact with the molten basalt.

We prefer this explanation for three reasons. First, the carbonate immediately beneath the basalt is greenish in color (suggesting the admixture of spalled basaltic glass fragments during rapid quenching, which have subsequently been altered to chlorite) and is

shattered into angular fragments intermixed with a basaltic breccia resembling a hyaloclastic texture (suggesting the rapid generation of steam). Second, the oxygen isotope compositions of carbonate sub-samples become progressively more negative approaching the basalt and into the diapirs and veins (Fig. 7), which are coarsely recrystallized and likely formed in the presence of very hot fluids. At Carter's Quarry, $\delta^{18}O$ values of the carbonates drop to as low as −14.0‰ directly beneath the two basalt levels. Similarly negative $\delta^{18}O$ values are not observed in the bedded carbonate above the lower basalt. This pattern of isotopic alteration is best explained by deposition of lava atop unconsolidated carbonate sediment causing isotopic modification, followed by later deposition of additional carbonate unaffected by the prior basaltic flow. Third, the coarse carbonate diapirs and veins are rimmed with garnet, which is notably not seen at the stratigraphic contact between basalt and carbonate. On the other hand, chlorite is present in the carbonate immediately underlying the basalt, but not in the diapirs and veins except along the rims co-occurring with garnet.

One explanation for the presence of garnet adjacent to the diapirs, but not at the base of the basalt, is a difference in fluid composition between the two locations. At a given pressure and temperature, the presence of a more H_2O-rich fluid with a lower X_{CO_2} within the diapirs (i.e. to the left of the $T - X_{CO_2}$ equilibria in Fig. 5A and B) would drive garnet-forming reactions A and B whereas a less H_2O-rich fluid with a higher X_{CO_2} at the base of the basalt (i.e. to the right of the equilibria in Fig. 5A and B) would not drive these reactions. We speculate that both the coarse carbonate and the garnet in and around the diapirs and veins might have formed as a result of flow of H_2O-rich pore fluid through them, including dissolved and particulate carbonate, resulting in a lower X_{CO_2} within the diapirs compared to the carbonate beds directly below the base of the basalt.

Recognition of a conformable relationship between the Catoctin volcanic rocks and the post-glacial cap carbonate at the top of the Fauquier Formation provides a means to radiometrically constrain this Ediacaran Period ice age. Zircons from a metarhyolite within the Catoctin from the Bluemont Quadrangle in northern Virginia previously yielded a 570 ± 12 Ma U–Pb discordia intercept age; zircons from a meta-rhyolite Catoctin flow from South Mountain in central Pennsylvania provided a discordia intercept age of 564 ± 9 Ma; and finally zircons from an extensive feeder dike to the Catoctin volcanic rocks gave a discordia intercept age of 572 ± 5 Ma (Aleinikoff et al., 1995). The large uncertainty on the age of the flow from Virginia stems from inheritance of older zircons; uncertainty about the validity of an assumption about the age of this older component led the authors to place only limited confidence in the calculated age. More recently, U–Pb TIMS zircon analyses of felsic tuffs intercalated with meta-basalt flows within 50 meters of the base of the formation provide an age of 571 ± 1 Ma (Southworth et al., 2009), which we accept as the most relevant age for deposition of the cap carbonate and glacial sediments of the underlying Fauquier Formation, based on our observations of soft-sediment deformation during emplacement of the volcanic rocks.

These age constraints clearly differentiate the Fauquier diamictites preserved in the upper Lynchburg Group from the 702–705 Ma glacial deposits in the Mechum River and Bunker Hill formations in the lower Lynchburg Group (Tollo and Hutson, 1996; Bailey and Peters, 1998). Furthermore, both of the better-constrained Catoctin ages are younger than the Gaskiers diamictite in Newfoundland (582 ± 0.4 Ma: Bowring et al., 2003) outside uncertainty, making the Fauquier ice age the youngest radiometrically constrained glaciation of the Ediacaran Period.

While more speculative, the intimate relationship of the Fauquier glacial deposits with the Catoctin flood basalt make it plausible that a rift-generated release of CO_2 to the atmosphere forced the end of this terminal Neoproterozoic ice age (Ganino and Arndt, 2009). Assuming an open hydrological cycle during this ice age and only moderately enhanced glacial albedo, only small to moderate increases in pCO_2 (3–4× present atmospheric level, Crowley et al., 2001) could have driven glacial termination.

5. Conclusions

Our observations of pillow basalt with chilled margins separated by ^{18}O depleted and highly recrystallized carbonate diapirs and veins, flame structures, and the hyaloclastic texture of mixed carbonate and volcanic lithologies at the Fauquier/Catoctin contact at Goose Creek support the conclusion that this boundary is conformable. This interpretation is further supported by the interleaving of marble and Catoctin volcanics at Carters Quarry where $\delta^{18}O$ values of the carbonate dive to negative extremes beneath (but not above) the flows. If correct, the age constraints for basal Catoctin volcanics (ca. 571 Ma) may be directly applied to the Fauquier cap carbonate and underlying glacial deposits.

Thus, radiometric constraints from Newfoundland and Virginia provide direct evidence for two discrete ice ages in the Ediacaran Period, although the global extent of these glaciations is presently difficult to assess. There are hints of even younger Ediacaran glaciations, including one near the Precambrian-Cambrian boundary (*cf.* Germs, 1974; Bertrand-Sarfati et al., 1995; Chumakov, 2009), which paints a broader picture of episodic ice ages throughout this tumultuous interval of Earth history.

Finally, the age constraint for the Fauquier glacial sequence opens a wider window into the relationship between glaciation and early metazoan evolution. Historically, the most complex examples of the Ediacaran biota were believed to have evolved millions of years after the last of the Neoproterozoic ice sheets melted. In Newfoundland, the Mistaken Point biota, including the cosmopolitan taxa *Charnia*, which is otherwise known only from the Avalon zone of central England, is preserved beneath ash layers in horizons spanning over 2000 m of section (Narbonne and Gehling, 2003). One of these ash layers in the Drook Formation immediately above the lowest occurrence of *Charnia* has been dated at 578.7 ± 0.4 Ma (Hoffman and Li, 2009); a second ash 1500 m higher within the fossiliferous Mistaken Point Formation is dated at 565 ± 3 Ma (Benus, 1988). These dates overlap with the age of the Fauquier glaciation. Accepting these constraints, it appears that Earth's earliest complex metazoans evolved in the midst of strong climatic oscillations potentially driven by the tectonic fragmentation of a supercontinent.

Acknowledgements

We wish to thank Laura (Baker) Hebert, Stacey Poulos, Christine (Missel) France, Taylor (Mauck) Johnston, Dan Earnest, David Johnston, Andrey Bekker, Frank Corsetti, Callan Bentley, Thomas Tamarkin, Scott Southworth, Russell Ashley, and Nick Collins for assistance in the field and in the stable isotope facility. In addition Jennifer Collins helped process the detrital zircon sample and acquire the U/Pb dates. George Gehrels and Victor Valencia enabled use of the MC-ICPMS at the University of Arizona. Supriya Khadke assisted with collection of powdered minerals for XRD analysis. We are indebted also to E-an Zen for his long-term interest in this project and insight on everything from map relations to metamorphic reactions and thermodynamics. Thanks also to editor Peter Cawood and to Alcides Sial and Juha Karhu for inviting this contribution to the special issue of Precambrian Research.

Appendix A. Supplementary data

Supplementary data associated with this article can be found, in the online version, at doi:10.1016/j.precamres.2010.07.008.

References

Aleinikoff, J.N., Zartman, R.E., Walter, M., Rankin, D.W., Lyttle, P.T., Burton, W.C., 1995. U–Pb ages of metarhyolites of the Catoctin and Mount Rogers formations, Central and Southern Appalachians; evidence for two pulses of Iapetan rifting. American Journal of Science 295, 428–454.

Alvarenga, C.J.S., Figueiredo, M.F., Babinski, M., Pinho, F.E.C., 2007. Glacial diamictites of Serra Azul Formation (Ediacaran, Paraguay belt): evidence of the Gaskiers glacial event in Brazil. Journal of South American Earth Sciences 23, 236–241.

Bailey, C.M., Peters, S.E., 1998. Glacially influenced sedimentation in the late Neoproterozoic Mechum River Formation, Blue Ridge province, Virginia. Geology 26, 623–626.

Badger, R.L., 1993. Fluid interaction and geochemical mobility in metabasalts: an example from the central appalachians. The Journal of Geology 101, 85–95.

Badger, R.L., Sinha, A.K., 1988. Age and Sr isotopic signature of the Catoctin volcanic province: implications for subcrustal mantle evolution. Geology 16, 692–695.

Banner, J.L., 1995. Application of the trace element and isotope geochemistry of strontium to studies of carbonate diagenesis. Sedimentology 42, 805–824.

Bao, H., Lyons, J.R., Zhou, C., 2008. Triple oxygen isotope evidence for elevated CO_2 levels after Neoproterozoic glaciation. Nature 453, 504–506.

Bartley, J.K., Pope, M., Knoll, A.H., Petrov, P.Y., Semikhatov, M.A., Sergeev, V.N., 1998. A Precambrian-Cambrian boundary succession from the western Siberian platform: geochemistry, stratigraphy, and paleontology. Geological Magazine 135, 473–494.

Benus, A.P., 1988. Sedimentological context of a deep-water Ediacaran fauna (Mistaken Point, Avalon Zone, eastern Newfoundland), In: Landing, E. et al., (Eds.), Trace Fossils, small shelly fossils and the Precambrian-Cambrian boundary. New York State Museum and Geological Survey Bulletin 463, pp. 8–9.

Berman, R.G., Brown, T.H., 1992. Thermobarometry with estimation of equilibration state [TWEEQU]: a software package for IBM or compatible personal computers. Geological Survey of Canada, Open File 2534 (ed. 1.02).

Bertrand-Sarfati, J., Moussine-Pouchkine, A., Amard, B., Ait-Kaci, A.A., 1995. First Ediacaran fauna found in western Africa and evidence for an Early Cambrian glaciation. Geology 23, 133–136.

Bowring, S., Myrow, P., Landing, E., Remezani, J., Grotzinger, J., 2003. Geochronological constraints on terminal Neoproterozoic events and the rise of metazoans. Geophysical Research Abstracts 5, 13219.

Bowring, S., Grotzinger, J.P., Condon, D.J., Ramezani, J., Newall, M., Allen, P.A., 2007. Geochronologic constraints of the chronostratigraphic framework of the Neoproterozoic Huqf Supergroup, Sultanate of Oman. American Journal of Science 307, 1097–1145.

Brown, W.R., 1970. Investigations of the sedimentary record in the Piedmont and Blue Ridge of Virginia. In: Fisher, G.W., et, al. (Eds.), Studies of Appalachian geology: Central and southern. Wiley-Interscience, New York, pp. 335–349.

Cawood, P.A., McCausland, P.J.A., Dunning, G.R., 2001. Opening Iapetus; constraints from the Laurentian margin in Newfoundland. Geological Society of America Bulletin 113, 443–453.

Cawood, P.A., Pisarevsky, S.A., 2006. Was Baltica right-way-up or upside-down in the Neoproterozoic? Journal of the Geological Society of London 163, 753–759.

Chumakov, N.M., 2009. The Baykonurian glaciohorizon of the Late Vendian. Stratigraphy and Geological Correlation 17, 373–381.

Condon, D., Zhu, M., Bowring, S., Wang, W., Yang, A., Jin, Y., 2005. U–Pb ages from the Neoproterozoic Doushantuo Formation, China. Science 308, 95–98.

Corkeron, M.L., George, A.D., 2001. Glacial incursion on a Neoproterozoic carbonate platform in the Kimberly region, Australia. Geological Society of America Bulletin 113, 1121–1132.

Crowley, T.J., Hyde, W.T., Peltier, W.R., 2001. CO_2 levels required for deglaciation of a "Near-Snowball" Earth. Geophysical Research Letters 28, 283–286.

Davis, A.M., Southworth, C.S., Reddy, J.E., 2001. Geologic map database of the Washington DC area featuring data from three 30×60 minute quadrangles; Frederick, Washington West, and Fredericksburg. U.S. Geological Survey Open File Report OFR-01-227.

Espenshade, G.H., 1986. Geology of the Marshall Quadrangle, Fauquier County, Virginia. U.S. Geological Survey Bulletin 1560, 60 pp.

Fike, D., Grotzinger, J., Pratt, L.M., Summons, R., 2006. Multi-stage Ediacaran ocean oxidation and its impact on evolutionary radiation. Geological Society of America Abstracts with Programs 28, 124–125.

Friedmann, S.J., Burbank, D.W., 1995. Rift basins and supradetachment basins: intracontinental extensional end-members. Basin Research 7, 109–127.

Ganino, C., Arndt, N.T., 2009. Climate changes caused by degassing of sediments during the emplacement of large igneous provinces. Geology 37, 323–326.

Gehrels, G.E., Valencia, V.A., Ruiz, J., 2008. Enhanced precision, accuracy, efficiency, and spatial resolution of U–Pb ages by laser ablation-multicollector-inductively coupled plasma-mass spectrometry. Geochemistry Geophysics Geosystems 9, Q03017, doi:10.1029/2007GC001805.

Germs, G.J.B., 1974. The Nama Group in south west Africa and its relationship to the Pan-African geosyncline. Journal of Geology 82, 301–317.

Grotzinger, J.P., Bowring, S.A., Saylor, B.Z., Kaufman, A.J., 1995. Biostratigraphic and geochronologic constraints on early animal evolution. Science 270, 598–604.

Halverson, G.P., Hoffman, P.F., Schrag, D.P., Maloof, A.C., Rice, H.N., 2005. Toward a Neoproterozoic composite carbon-isotope record. Geological Society of America Bulletin 117, 1181–1207.

Hayes, J.M., Kaplan, I.R., Wedeking, K.W., 1983. Precambrian organic geochemistry; preservation of the record. In: Schopf, J.W. (Ed.), Earth's Earliest Biosphere, its Origin and Evolution. Princeton University Press, Princeton, pp. 93–132.

Hoffman, P.F., Kaufman, A.J., Halverson, G.P., Schrag, D.P., 1998. A Neoproterozoic snowball earth. Science 281, 1342–1346.

Hoffman, P.F., Schrag, D.P., 2002. The snowball Earth hypothesis: testing the limits of global change. Terra Nova 14, 129–155.

Hoffman, P.F., Li, Z.-X., 2009. A palaeogeographic context for Neoproterozoic glaciation. Palaeogeography, Palaeoclimatology, Palaeoecology 277, 158–172.

Hoffmann, K.-H., Condon, D.J., Bowring, S.A., Crowley, J.L., 2004. U–Pb zircon date from the Neoproterozoic Ghaub Formation, Namibia: constraints on Marinoan glaciation. Geology 32, 817–820.

Holland, T.J.B., Powell, R., 1998. An internally consistent thermodynamic data set for phases of petrological interest. Journal of Metamorphic Geology 16, 309–343.

Jacobsen, S.B., Kaufman, A.J., 1999. The Sr, C and O isotopic evolution of Neoproterozoic seawater. Chemical Geology 161, 37–57.

Jiang, G., Kaufman, A.J., Christie-Blick, N.J., Zhang, S., Wu, H., 2007. Carbon isotope variability across the Ediacaran Yangtze platform in South China: implications for a large surface-to-deep ocean $\delta^{13}C$ gradient. Earth and Planetary Science Letters 361, 303–320.

Kasselas, G.D. 1993, Stratigraphic framework, structural evolution and tectonic implications of the eastern Blue Ridge sequence in the Central Appalachians near Warrenton, Virginia. Virginia Polytechnic Institute Masters Thesis. 117 pp.

Kasselas, G.D., Glover, L. III, 1997. Late Proterozoic cover rocks in the Blue Ridge of Virginia; Do they include a terrane boundary?, In: Glover, L. III, Alexander, E., (Eds.), Central and Southern Appalachian sutures; results of the EDGE Project and related studies. Geological Society of America – Special Paper 314, pp. 89–105.

Kaufman, A.J., Hayes, J.M., Knoll, A.H., Germs, G.J.B., 1991. Isotopic compositions of carbonates and organic carbon from Upper Proterozoic successions in Namibia: stratigraphic variation and the effects of diagenesis and metamorphism. Precambrian Research 49, 301–327.

Kaufman, A.J., Jacobsen, S.B., Knoll, A.H., 1993. The Vendian record of C- and Sr-isotopic variations: implications for tectonics and paleoclimate. Earth and Planetary Science Letters 120, 409–430.

Kaufman, A.J., Knoll, A.H., 1995. Neoproterozoic variations in the C-isotopic composition of seawater: stratigraphic and biocgeochemical implications. Precambrian Research 73, 27–49.

Kaufman, A.J., Knoll, A.H., Narbonne, G.M., 1997. Isotopes, ice ages, and terminal Proterozoic earth history. Proceedings of the National Academy of Sciences of the United States of America 94, 6600–6605.

Kaufman, A.J., Corsetti, F.A., Varni, M.A., 2007. The effect of rising atmospheric oxygen on carbon and sulfur isotope anomalies in the Neoproterozoic Johnnie Formation, Death Valley, USA. Chemical Geology 237, 47–63.

Kennedy, M.J., 1996. Stratigraphy, sedimentology, and isotopic geochemistry of Australian Neoproterozoic postglacial cap dolostones: deglaciation, $\delta^{13}C$ excursions, and carbonate precipitation. Journal of Sedimentary Research 66 (6), 1050–1064.

Kline, S.W., Lyttle, P.T., Schindler, J.S., 1991. Late Proterozoic sedimentation and tectonics in Northern Virginia: Geologic Evolution of the Eastern United States, Field Trip Guide Book, NE-SE GSA 1991. VMNH Guidebook 2, pp. 263–294.

Li, Z.X., Bogdanova, S.V., Collins, A.S., Davidson, A., De Waele, B., Ernst, R.E., Fitzsimons, I.C.W., Fuck, R.A., Gladkochub, D.P., Jacobs, J., Karlstrom, K.E., Lu, S., Natapov, L.M., Pease, V., Pisarevsky, S.A., Thrane, K., Vernikovsky, V., 2008. Assembly, configuration, and breakup history of Rodina; a synthesis. Precambrian Research 160, 179–210.

Liu, P., Yin, C., Gao, L., Tang, F., Chen, S., 2009. New material of microfossils from the Ediacaran Doushantuo Formation in the Zhangcunping area, Yichang, Hubei Province and its zircon SHRIMP U–Pb age. Chinese Science Bulletin 54, 1058–1064.

Martin, M.W., Grazhdankin, D.V., Bowring, S.A., Evans, D.A.D., Fedonkin, M.A., Kirschvink, J.L., 2000. Age of Neoproterozoic bilatarian body and trace fossils, White Sea, Russia: implications for metazoan evolution. Science 288, 841–845.

McFadden, K.A., Huang, J., Chu, X., Jiang, G., Kaufman, A.J., Zhou, C., Yuan, X., Xiao, S., 2008. Pulsed oxidation and biological evolution in the Ediacaran Doushantuo Formation. Proceedings of the National Academy of Sciences of the United States of America 105, 3197–3202.

Meert, J.G., Van der Voo, R., Payne, T.W., 1994. Paleomagnetism of the Catoctin volcanic province; a new Vendian-Cambrian apparent polar wander path for North America. Journal of Geophysical Research 99, 4625–4641.

Myrow, P., Kaufman, A.J., 1999. A newly-discovered Neoproterozoic cap carbonate atop the glaciogenic Gaskiers Formation, Newfoundland, Canada. Journal of Sedimentary Research 69, 784–793.

Narbonne, G.M., Gehling, J.G., 2003. Life after snowball; the oldest complex Ediacaran fossils. Geology 31, 27–30.

Parker, P.E., 1968. Geologic investigation of the Lincoln and Bluemont Quadrangles, Virginia. Virginia Division of Mineral Resources, Report of Investigations 14, 23 pp.

Pelechaty, S., Kaufman, A.J., Grotzinger, J.P., 1996. Evaluation of $\delta^{13}C$ isotope stratigraphy for intrabasinal correlation: data from Vendian strata of the Olenek uplift and Kharaulakh Mountains, Siberian platform, Russia. The Bulletin of the Geological Society of America 108, 992–1003.

Pisarevsky, S.A., Komissarova, R.A., Khramov, A.N., 2000. New paleomagnetic result from Vendian red sediments in Cisbaikalia and the problem of the relationship of Siberia and Laurentia in the Vandian. Geophysical Journal International 140, 598–610.

Reed Jr., J.C., 1955. Catoctin Formation near Luray, Virginia. Bulletin of the Geological Society of America 66, 871–896.

Saylor, B.Z., Kaufman, A.J., Grotzinger, J.P., Urban, F., 1998. A composite reference section for terminal Proterozoic strata of southern Namibia. Journal of Sedimentary Research 68, 1223–1235.

Southworth, S., Burton, W.C., Schindler, J.S., Froelich, A.J., 2006. Geologic map of Loudoun County, Virginia. U.S. Geological Survey Geologic Investigations Series Map I–2553, scale 1:50,000, 34 pp. text.

Southworth, C.S., Brezinski, D.K., Drake, A.A., Burton, W.C., Orndoff, R.C., Froelich, A.J., Reddy, J.E., Denenny, D., and Daniels, D.L., 2008. Geologic map of the Frederick 30' X 60' quadrangle, Maryland, Virginia, and West Virginia. U.S. Geological Survey, Scientific Investigations Map SIM-2889.

Southworth, S., Tollo, R.P., Aleinikoff, J.N., Bailey, C., Burton, W.C., Crider, E., Hackley, P.C., Kunk, M.J., Mundil, R., Naeser, C.N., Naeser, N., and Smoot, J., 2009. New geologic map and geochronology of the Shenandoah National Park region, Virginia. Geological Society of America Abstracts with Programs 41, 365.

Thompson, M.D., Bowring, S.A., 2000. Age of the Squantum "tillite", Boston Basin, Massachusetts; U–Pb zircon constraints on terminal Neoproterozoic glaciation. American Journal of Science 300, 630–655.

Tollo, R.P., Hutson, F.E., 1996. 700 Ma rift event in the Blue Ridge Province of Virginia; a unique time constraint on pre-Iapetan rifting of Laurentia. Geology 24, 59–62.

Wehr, F., 1985. Stratigraphy of the Lynchburg Group and Swift Run Formation. Southeastern Geology 25, 225–239.

Wehr, F., Glover, L., 1985. Stratigraphy and tectonics of the Virginia-North Carolina Blue Ridge; evolution of a late Proterozoic-early Paleozoic hinge zone. Geological Society of America Bulletin 96, 285–295.

Wehr, F., 1986. A proglacial origin for the upper Proterozoic Rockfish Conglomerate, central Virginia, U.S.A. Precambrian Research 34, 157–174.

Xiao, S., Bao, H., Wang, H., Kaufman, A.J., Zhou, C., Li, G., Yuan, X., Ling, H., 2004. The Neoproterozoic Quruqtagh Group in eastern Chinese Tianshan: evidence for a post-Marinoan glaciation. Precambrian Research 130, 1–26.